INSTITUTE OF PHYSICS PUBLISHING PHYSIOLOGICAL MEASUREMENT

Physiol. Meas. **25** (2004) 421–436 PII: S0967-3334(04)70867-9

A new biomedical sensor for measuring PCO_2

Peyman Mirtaheri[1,2,4], **Sverre Grimnes**[2,4], **Ørjan G Martinsen**[2] **and Tor Inge Tønnessen**[1,3]

[1] Interventional Center, Rikshospitalet University Hospital, Norway
[2] Department of Physics, University of Oslo, PB 1048 Blindern, Norway
[3] Department of Anesthesiology, Rikshospitalet University Hospital, Norway
[4] Department of Clinical and Biomedical Engineering, Rikshospitalet University Hospital, Norway

Received 22 October 2003, accepted for publication 22 December 2003
Published 16 February 2004
Online at stacks.iop.org/PM/25/421 (DOI: 10.1088/0967-3334/25/2/002)

Abstract

Measuring PCO_2 (partial pressure of carbon dioxide) in an organ can enable early detection of ischemia. However, there are few clinical applicable solutions for measuring PCO_2. Based upon the requirement for clinical applications, a conductivity based PCO_2 sensor is proposed. A conductivity based PCO_2 sensor measures conductance in an aqueous solution separated from the measured object by a gas-permeable membrane. A bridge design with two cavities is favored for such a sensor. A planar and a cylindrical macro prototype based upon the bridge design were studied. The design criteria were based on the contribution from the electrode polarization, stray capacitances, contact area with the sample and design ability to miniaturize the sensor. The cylindrical sensor is favored because of its large contact area and advantages for miniaturization. Further investigation has to be done to confirm the functionality of such a design in a miniaturized form and its clinical performance.

Keywords: biomedical sensor, ischemia, PCO_2, gas measuring, conductivity

1. Introduction

The transport of oxygen to the mitochondria inside each individual cell is a prerequisite for aerobic metabolism. Decreasing oxygen delivery (DO_2) below a critical value, by occlusion of the arteries, shock, severe anemia or hypoxia will result in an anaerobic condition. The cells of an organ cannot tolerate this condition for an extended time. If the underlying problem is not corrected, it may cause irreversible damage to the organ. Except for the beating heart and the conscious brain, organ ischemia is not detected in real time. Liver and kidney can be severely ischemic without any symptoms before the organ damage is irreversible. Thus, there

is a clinical need for methods to detect ischemia in symptomatically silent organs. On the basis of our own research (Tønnessen and Kvarstein 1996, Tønnessen 1997, Kvarstein *et al* 2004) and in addition to results from several other groups (Hoffman *et al* 1998, Hong 1996), we are confident that measuring PCO_2 (partial pressure of carbon dioxide) in the organ is a sensitive marker for early detection of ischemia.

Despite increased research activity in the area of sensor development, there are still few available solutions for measuring PCO_2 in organs. These existing solutions are limited and troublesome to apply in clinical applications (Rolfe 1995). Disadvantages such as inability for miniaturization or a cost that is too high for routine clinical use, underline the need for developing a new type of sensor (Siggaard-Andersen *et al* 1995). There are several solutions for *in vitro* measurements such as in blood gas machines, where usually a chemical or an optical PCO_2 sensor is used. However, they are difficult to apply for the clinical real-time measurements.

The basic principle of a PCO_2 sensor has been unchanged since it was first reported by Stow *et al* (1957) and then further developed by Severinghaus and Brandley (1958). The sensor had a gas-permeable membrane with a thin liquid film positioned behind it. In the liquid film, the water will dissociate the CO_2 which diffuses into the measuring chamber through the membrane until the equilibrium state is achieved (Nunn 1993). The traditional Stow–Severinghaus sensor measures the pH changes in the measuring chamber.

A conductivity based PCO_2 sensor may have several advantages over other measuring principles (Kempen and Kreuzer 1975). The sensor measures conductance in an aqueous solution separated from the measured object by a gas-permeable membrane. The ion formation in the aqueous solution is proportional to the root of the partial pressure of carbon dioxide (Koryta *et al* 1993). The total conductance G_e can be calculated by

$$G_e = \Psi * \left\{\sigma_0 + \left(\Lambda_{H^+}\vartheta_{H^+} + \Lambda_{HCO_3^-}\vartheta_{HCO_3^-}\right)(KK_H PCO_2)^{1/2}\right\}$$

where the constant Ψ (m) is the geometrical factor and is equal to the area divided by the length of the measuring cell, σ_0 (S m^{-1}) is the conductivity when the PCO_2 is 0 kPa, Λ (m^2 (Ω mol)$^{-1}$) is the molar conductivity of ions, ϑ (unitless) is the activity of ions in the solutions, K (mol l^{-1}) is the activity coefficient and K_H (mol (l kPa)$^{-1}$) is Henry's constant.

The basic structure of the new conductivity based PCO_2 sensor is simple: two electrodes and a closed water-filled chamber.

Nevertheless, conductivity measurements would not be ideal and could be troublesome if one is not able to control errors from electrode polarization, stray capacitance, contamination, pressure and temperature. In the present study, we evaluate different design solutions concerning the aforementioned sources of error. Two design solutions were developed to prepare for future miniaturized designs. The sensor design criteria were based on contact area with the sample, ability to miniaturize the sensor, production complexity and ease of application.

2. Methods and results

2.1. Electrical simulations

2.1.1. Electrical equivalent model. Based on previous studies (Lis *et al* 1979, Baker *et al* 1996, Varlan and Sansen 1997) a conductivity sensor has been investigated with different designs. The common feature of these designs is that they all have two electrodes placed in a small cavity filled with an aqueous solution.

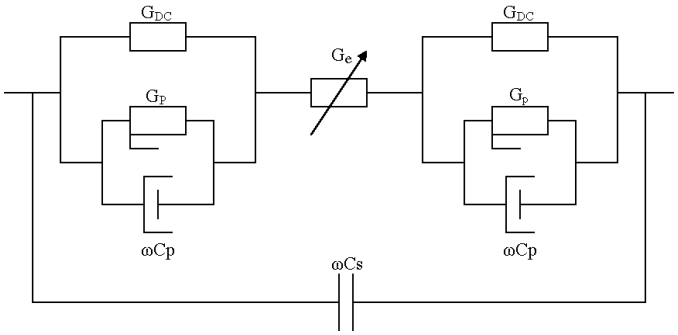

Figure 1. Electrical model for the PCO_2 sensor. G_p and C_p are frequency-dependent components.

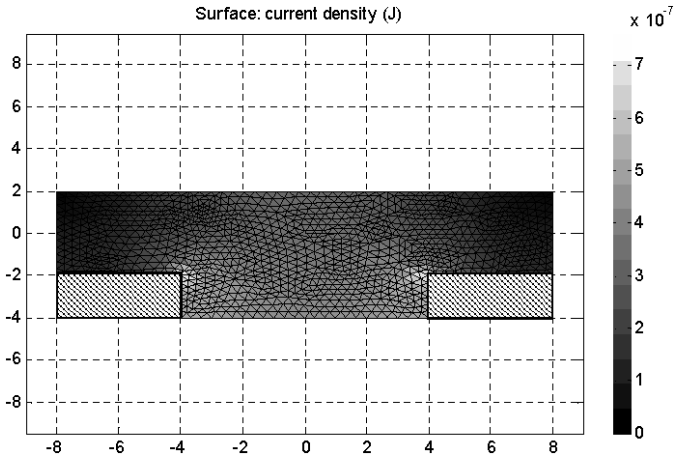

Figure 2. Current density field inside a single water-filled cavity with two electrodes.

An electrical model for the sensor illustrates the components that influence the measurement results (figure 1). A direct measurement of G_e, which is the conductance of the electrolyte in the measuring cavity, would be an ideal measurement. In reality, however, other components such as electrode polarization immittance (G_p, C_p and G_{dc}) and stray capacitance (C_s) also contribute to the measuring result.

The electrode polarization immittance, which is discussed later in this paper, is influenced by the electrode material, concentration of the electrolyte, temperature and contact area. The larger the contact area, the less is the effect of electrode polarization on the measurements (Grimnes and Martinsen 2000, Schwan 1968).

2.1.2. Current density field simulations. The simulations shown were performed with Femlab (version 2.3, Comsol Inc.).

One cavity and two electrodes. Figure 2 shows the current density field for a single cavity design. The electrode polarization is inversely proportional to the electrode surface area. With an uneven current density distribution, the effective electrode area will be less than the actual electrode area. Therefore, the single cavity design is not a preferred design.

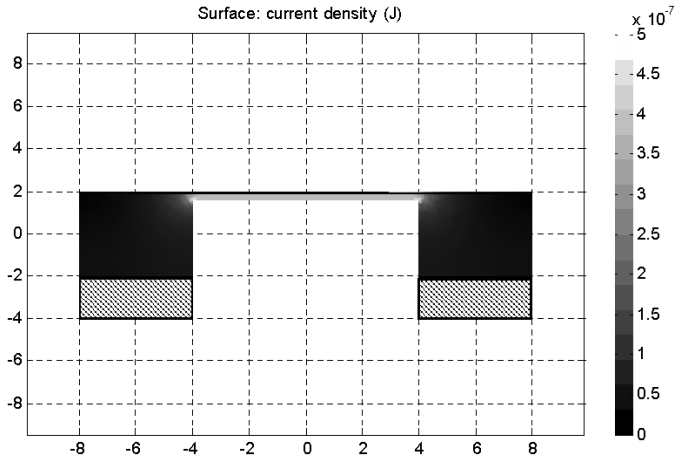

Figure 3. Current density field with a bridge and two cavities.

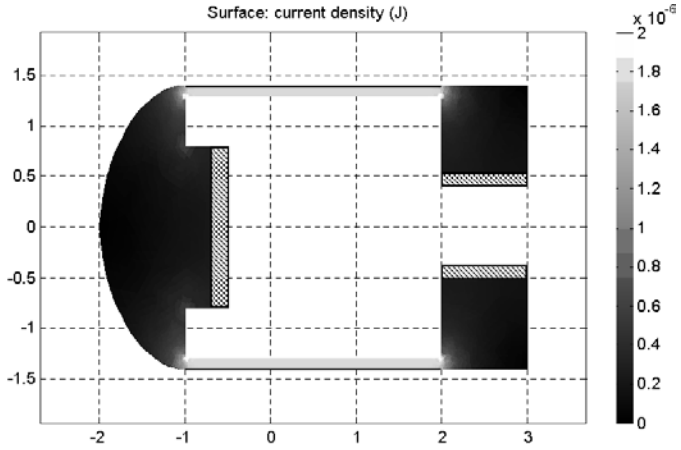

Figure 4. Current density field for the cylindrical shaped sensor.

Two cavities and a connecting bridge. When the electrodes are placed in two separate cavities with a connecting thin liquid bridge, a very even current density field will be achieved which utilizes the electrode surface area effectively (figure 3). The main advantage of this design is that the contribution from electrode polarization is minimized. This planar model is further investigated in section 2.2.

Since a future catheter design was of interest, we transformed the planar design into a cylindrical shape (figure 4). The same even current density distribution was obtained at the electrode surface area. The cylindrical model is further investigated in section 2.3.

2.2. Planar design

Figure 5 illustrates the planar design for a macro prototype. The planar designs with silicon (Si), much used by electronic industries, have evolved from the micromachining technology (Jacobs *et al* 1995). Its application and cost effectiveness in sensor production are significant. However, we chose to manufacture the sensor body of polymethyl methacrylate (PMMA)

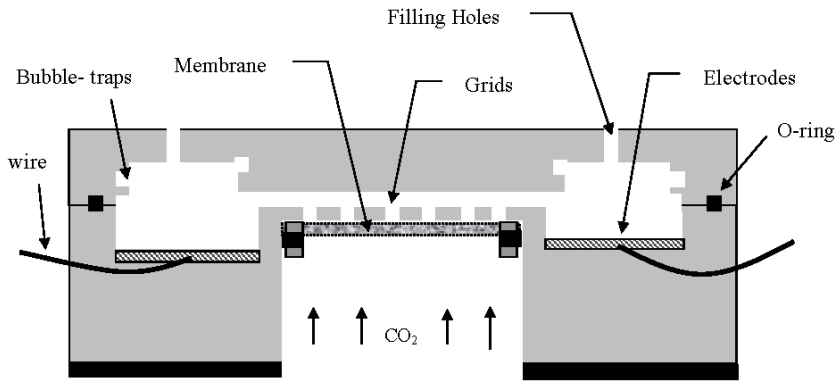

Figure 5. The planar design with dimensions of 2 × 1 × 1 cm.

rather than silicon. Silicon is a semiconductor, and has to be covered by a SiO_2 layer. Such a layer is susceptible to water absorption and instability.

A fully automatic milling machine (FP3A, Deckel Eurostandard) was applied to manufacture the sensor body. It can manufacture complex planar geometries with an error down to 5 μm if the material and the working temperature are stable. The sensor was produced in two halves. On the lower part of the cavities, electrodes and the membrane with supporting grid were placed. The upper part was designed to cover the bridge channel, with filling holes and a sealing lid. The cross section and the length of the channel were 1 mm × 4 mm and 8 mm respectively, corresponding to $\Psi = 0.5 \times 10^{-3}$ m. The diameter of the cavities was 4 mm (figure 7). The membrane was a 100 μm thick polytetrafluoroethylene (PTFE) film. It was pulled on a PMMA ring and fixed by a rubber O-ring. The grid supported the membrane mechanically making sure that the measuring channel geometry was stable.

Based on the results from section 2.4.2, silver was chosen as the electrode material. The two disk-shaped electrodes were 4 mm in diameter and 1 mm thick. The electrodes were connected to external wires by a conductive glue (Conductive epoxy CW2400, Chemtronics). The circumference of the disk electrodes was further covered with light-curing glue (Acrifix 192, Röhn, GmbH). The reason for this is elaborated in section 2.4.5.

All parts of the sensor were cleansed with Triton X100 (Sigma Chemical, USA) to remove undesired ions. The sensor was filled by injecting de-ionized water with a 1 ml syringe through one of the filling holes. The applied de-ionized water manufactured by Electrolube (Berkshire, UK) had conductivity in the range of 4–15 μS cm^{-1}. After the filling was finished and no bubbles were observed inside the measuring chamber, the lid system was drawn over the filling holes to seal off the sensor.

2.3. Cylindrical design

In recent years, there has been new activity in the field of miniaturization with polymers where complex structures can be achieved with remarkable precision (Detemple *et al* 1998, Niggermann *et al* 1999).

The cylindrical design was producible either by an injection molding processes or by mechanical turning. We chose the mechanical turning. The sensor body was made of PMMA with a diameter of 2.8 mm. The PTFE membrane was manufactured as a hollow cylinder with an outer diameter and wall thickness of 3.3 mm, 150 μm respectively, corresponding to $\Psi = 0.8 \times 10^{-3}$ m. A large filling hole was drilled at the top of the membrane. To make the

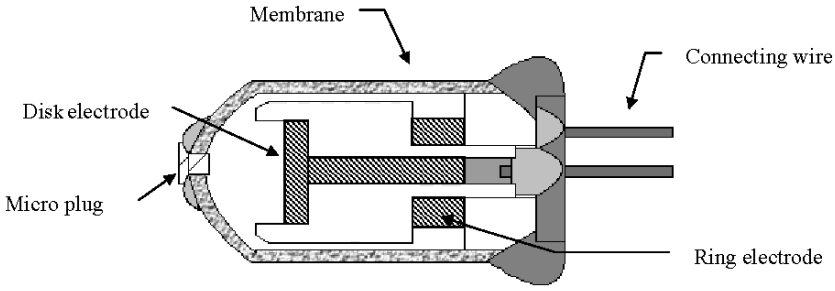

Figure 6. Cylindrical design with an outer diameter of 3.4 mm and a length of 6.8 mm.

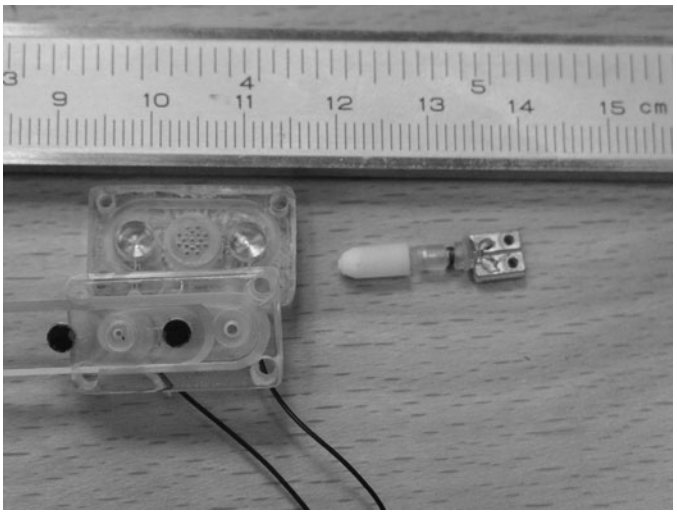

Figure 7. The planar (left) and cylindrical (right) sensors.

sensor less pressure sensitive and more robust, a rather thick membrane was chosen. Figure 6 illustrates the sensor structure.

The electrodes were made of silver and designed in two different shapes: ring and disk shaped. We glued the electrode circumference with the light-curing glue. The electrodes were further connected to 150 μm diameter wires by the conductive glue. The tiny connective wires were mechanically fragile, therefore a small PCB board was glued at the back end and then tiny wires were connected to it. We soldered thicker and mechanically stronger wires from the PCB board to the instruments.

We attempted to glue the membrane to the sensor body but the PTFE was a difficult material to glue. A 'primer' suggested by Loctite (Loctite 770) makes it possible to glue PTFE to other materials. However, our experience with the primer was that the membrane properties also changed dramatically. The PTFE membrane became more permeable to ions, which increased the chance of drifting. We concluded that a mechanical tight sealing with a combination of hot glue (Gluematic, Germany) could solve the problem.

Before the assembly of the sensor, all parts were cleansed with Triton X100. The sensor was filled with a small syringe containing the de-ionized water. The filling hole was sealed by inserting a PTFE plug fixed with hot glue. Hot glue was preferred in order to close the gap quickly without contaminating the de-ionized water.

Figure 7 shows an actual image of both sensors.

2.4. Sensors' characteristics

2.4.1. Instrumentation. A lock-in amplifier (SR830, Stanford Research) was utilized for testing the sensors except for the case in section 2.4.3. We measured admittance by applying an amperometric method with constant voltage amplitude and the corresponding current measured. The impedance of the electrode/electrolyte interface can change with the amplitude of the measuring signal (Ragheb and Geddes 1990). According to the experimental results of Onaral and Schwan (1982), the onset of nonlinearity appears virtually independent of frequency and occurs near an overpotential of 100 mV. On the other hand, small sine signals are difficult to detect due to poor signal/noise ratio. The voltage output amplitude was therefore chosen to be 60 mV rms and the chosen measuring frequency was 700 Hz (cf section 2.4.4).

During the testing, the internal sine signal oscillator of the lock-in amplifier was fed directly to the sensor. The sensor output was then connected through a preamplifier to convert the electrode current into a voltage. In addition, the preamplifier contained a feedback circuit to minimize any dc current between the electrodes. A DC current causes polarization, which may cause drifting.

2.4.2. Measured electrode polarization. Four sensors with the chosen planar geometry but different electrode materials were examined. The chosen metals were gold, platinum, silver and medical stainless steel. The gold, platinum and silver metals had impurity less than 1 ppm (Rasmussen AS, Norway). The sensors were filled with 3.08 mM NaCl solution. The expected serial resistance of the solution was calculated and subtracted from the total measured impedance to achieve the electrode polarization impedance (figure 1). The electrode polarization impedance/phase shift versus frequency is presented in figure 8. The contribution of electrode polarization for the stainless steel was so large that we decided to exclude this metal from further use. The results also showed that the silver, gold and platinum electrodes have the smallest phase shift and polarization impedance. We chose silver since it was easier for mechanical turning and less expensive. These results are a part of a larger study that will be presented separately.

2.4.3. Impedance analysis of the sensors. To make the analysis of the sensor impedance easier, we applied an impedance/gain-phase analyzer system (model 1260+1294 Solatron instruments). The length of connective wires did not exceed 50 cm. The sensors were tested both empty and filled with de-ionized water. The impedance and the phase shift were then plotted as a function of frequency (see figure 9). The capacitance value for the empty cell could be calculated and was 6 pF and 8 pF for the planar sensor and cylindrical shaped sensor, respectively. The filled sensor's impedance did not change with frequency up to a point where the stray capacitance's influence on measurements became significant.

2.4.4. Optimal measuring frequency. Figure 8 shows that the electrode polarization impedance and the phase shift are small for frequencies above 100 Hz. Increasing the contribution of the electrode polarization will cause larger error (cf figure 1). At high frequencies (figures 8 and 9), the effect of the stray capacitances became dominant. For example, calculations from data in figure 9(a) show that the total stray susceptance of the sensor will be more dominant than its conductance at frequencies above 13 kHz. In order to handle a large range of stray capacitances, we chose to use a much lower frequency. We concluded that satisfactory measurements could be achieved in the frequency range 200–1000 Hz and chose the frequency of 700 Hz for all measurements.

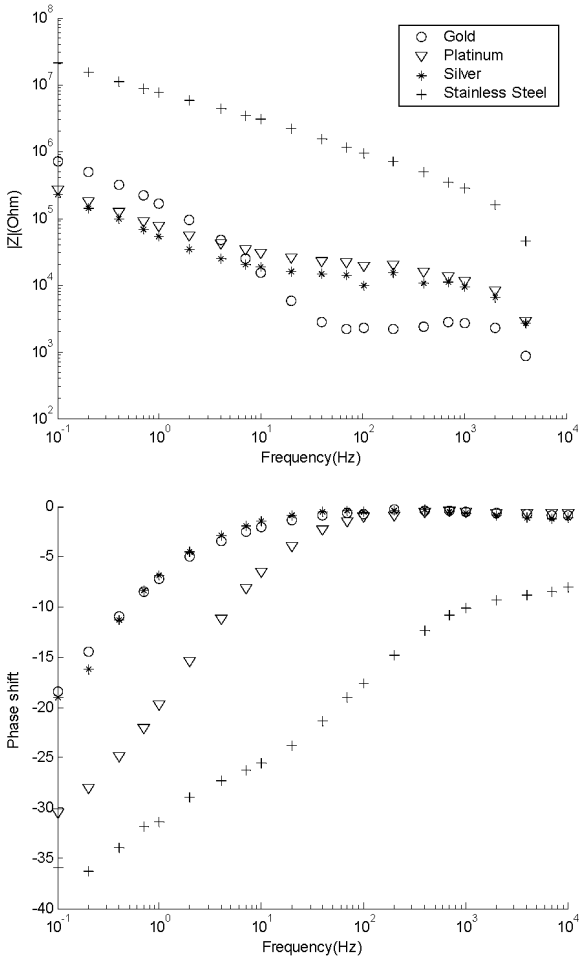

Figure 8. Electrode polarization impedance (superior) and phase shift (inferior) of the planar sensor with different electrode materials in 3.08 mM NaCl solutions.

2.4.5. Drifting. An internal drift will occur if the electrodes, sensor body or membrane presents ions to the de-ionized water. When the planar sensor was placed in de-ionized water and tested in time, increased baseline values were detected (see figure 10). This must have been due to an increase of ion concentration from internal sources. The conductive glue was therefore the most probable source. We tried to cover it with the Acryfix. The outcome was compared with the previous results (figure 10). The figure shows that the conductive glue even when completely cured, gave ion extracts into the de-ionized water. Accordingly, both sensor prototypes were treated with Acryfix to cover all conductive glue surfaces.

2.4.6. Pressure sensitivity. The stability of the channel geometry and the sealing of the sensor were tested by placing the sensor at the bottom of a cylindrical shaped water tank filled gradually with 0.9% NaCl solution. The moment the output value changed more than 10% of its baseline value, the level of the water tank was noted. Both sensors started to drift when the pressure exceeded 70 cm H_2O and 50 cm H_2O for planar and cylindrical sensors,

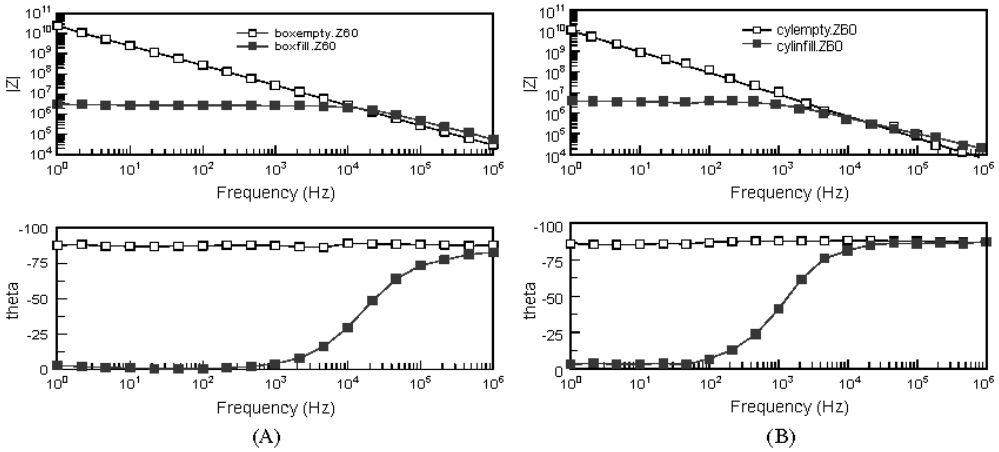

Figure 9. Impedance and phase shift for planar (A) and cylindrical (B) sensors when empty (open squares) and filled with de-ionized water (filled squares).

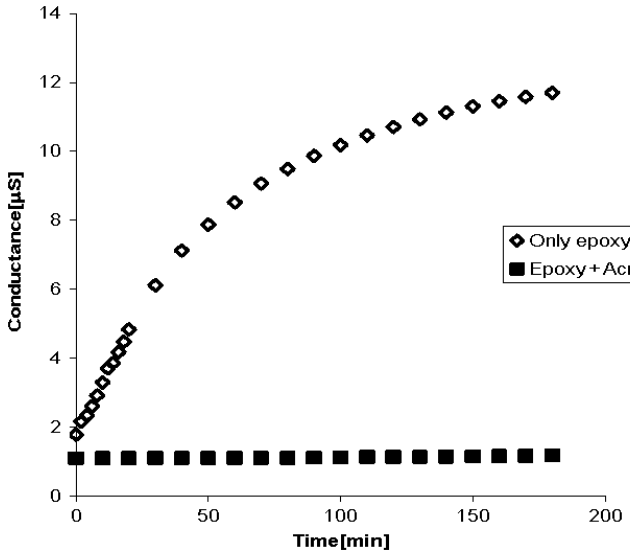

Figure 10. Internal drifting of the planar sensor when glued by conductive epoxy and when covered by the Acrifix.

respectively. Since the output value increases, the pressure sensitivity must be due to a rupture of the sealing.

2.4.7. Membrane properties. If the membrane were permeable to ions, an external drift or pressure sensitivity would occur. To investigate the membrane structure, SEM images of the membranes surfaces were taken by a scanning electron microscope (Philips XL-30). The images are presented in figures 11 and 12.

2.4.8. Time constant. The sensors were tested by submerging them into a solution with 6 kPa PCO_2 gas until the equilibrium was achieved. The PCO_2 solution was then replaced

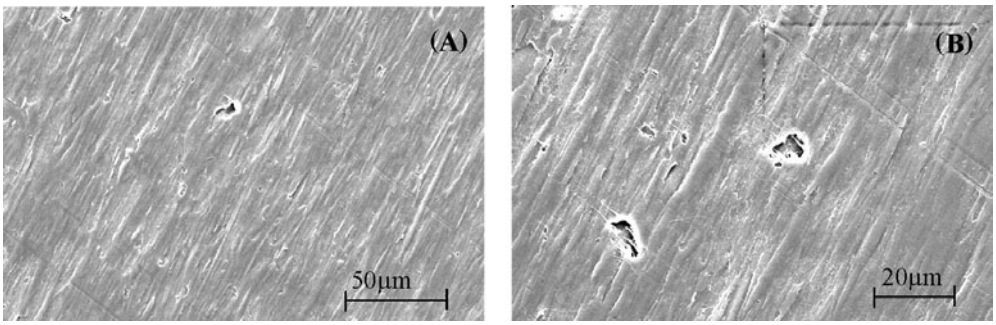

Figure 11. SEM images showing two different locations at the flat sheet membrane, magnified 1000X (A) and magnified 2000X (B).

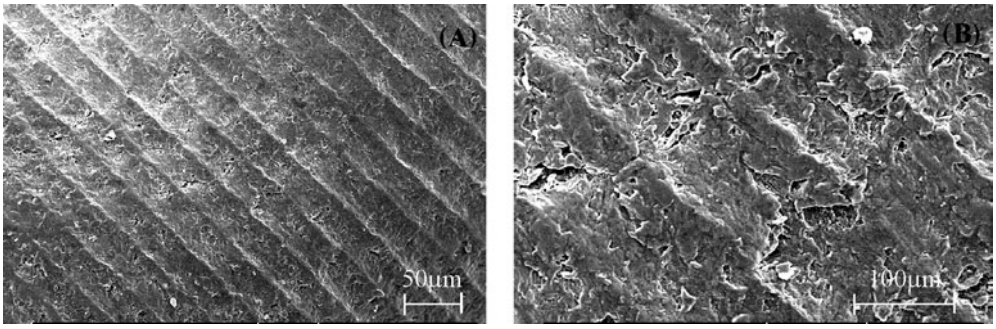

Figure 12. SEM images of the cylindrical membrane magnified 150X (A) and magnified 500X (B).

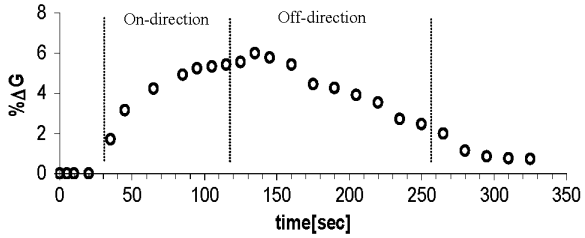

Figure 13. A typical example of response time for the planar sensor.

with de-ionized water and the measurements continued. The conductance measurements enabled us to calculate the sensor's time constant that is 63.2% of the maximum conductance changes. Figure 13 shows a typical example of the time constant for the planar sensor. The average time constant for the planar sensor was about 45 s for the on-direction and 88 s for the off-direction. Since the cylindrical sensor had a thicker membrane, the response time was longer. The average time constant was about 48 s for the on-direction and 130 s for the off-direction.

2.4.9. Calibration curves. The PCO_2 testing of the sensors was carried out by submerging the sensors in water-filled bottles with different CO_2 gas tensions. To avoid any leakage problem, both sensors were not submerged more than 1 cm into the water.

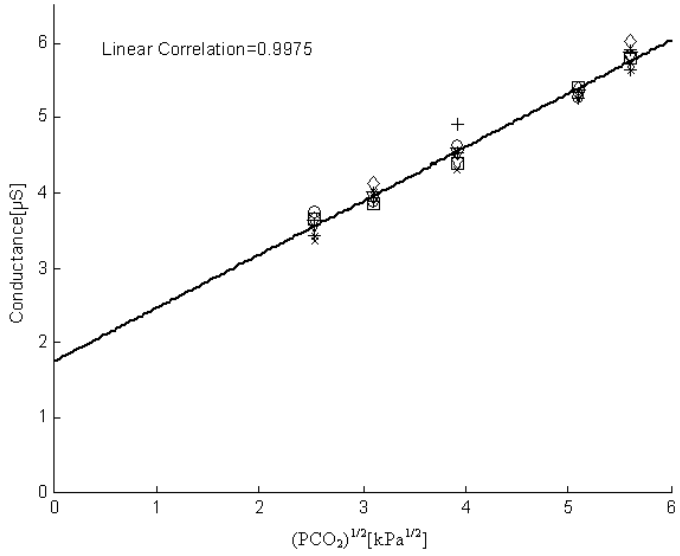

Figure 14. Measured conductance with planar sensor versus $(PCO_2)^{1/2}$ ($kPa^{1/2}$) repeated in time.

Bottles containing 1 litre of sterile water were bubbled for a certain time with 100% CO_2 gas. The gas tension of each bottle was then tested against a blood gas analyzer (ABL650, Radiometer AS, Denmark). ABL650 was calibrated 30 min before the experiments were started and the calibration error was not more than 1 kPa.

The temperature was kept constant at 23 °C during the experiments by placing the bottles in a circulated water bath (Kebolab, Norway). The ABL650 measures all the blood gas tensions at 37 °C. Therefore, the PCO_2 measurements by ABL650 were converted according to the temperature of the experimental setup.

The measured conductance values were plotted against the gas tensions in each bottle. The measurements on sensors were repeated six times in a period of 1 hr and 30 min to detect any measuring error in time. Figures 14 and 15 show the measured conductances as a function of PCO_2.

3. Discussion

3.1. The time constant and the membrane

The permeation rate of CO_2 through a gas-permeable membrane depends mostly on the membrane permeability, in addition to the temperature, and the pressure differences across the membrane.

The membrane thickness, membrane physical properties, electrolyte volume and the ionic reaction speed in the electrolyte have an effect on the sensor's time constant. As suggested by Varlan and Sansen (1997), the time constant of the membrane and electrolyte can roughly be calculated by $\frac{d_m^2}{D_m} + \frac{l^2}{D_e}$, where d_m is the thickness of the membrane and l is called the aspect ratio defined as the ratio of the active electrolyte volume per membrane area. D_m and D_e are the diffusion coefficients for the membrane and de-ionized water, respectively.

For PTFE, the diffusion coefficient is variable and dependent on the nano-porous structure of the material. The estimated value is between 5×10^{-6} and 5×10^{-5} $cm^2\ s^{-1}$

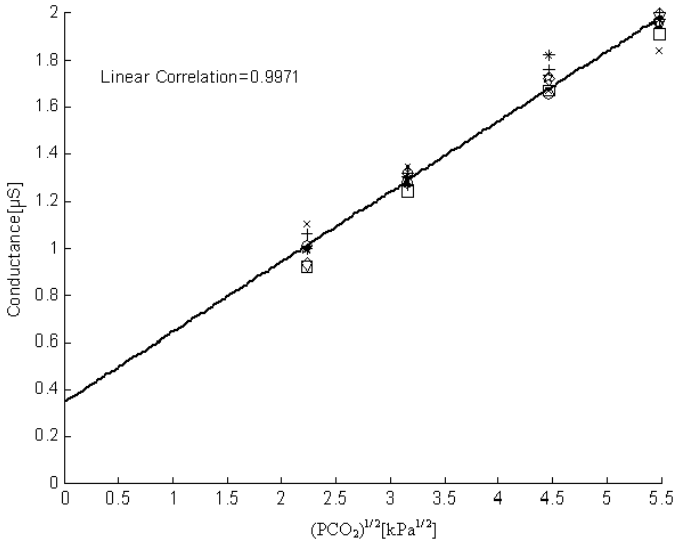

Figure 15. Measured conductance with cylindrical sensor versus $(PCO_2)^{1/2}$ ($kPa^{1/2}$) repeated in time.

(Cunningham and Williams 1980). For de-ionized water, the diffusion coefficient is 2.5×10^{-5} cm^2 s^{-1}. For the planar sensor, the calculated response time is about 50 s where only 40% of the value was contributed by the membrane. For the cylindrical sensor, we have a very small aspect ratio and therefore the diffusion time through the membrane dominates the response time. For a PTFE membrane with a thickness of about 150 μm, we could expect a time constant of about 45 s. The values that we measured for the on-direction of the time constants were close to the calculated values. However, the off-direction time constants were longer because of the slow chemical processes transferring protons and bicarbonates into CO_2 (Kempen and Kreuzer 1975).

When we tested the sensors for the external pressures, the results showed that the sensors were incapable of working at pressures larger than 50–80 cm H_2O. This makes the sensors susceptible in rough environments such as the beating heart or contracted muscle.

We suspected that the membranes were not fully tight and investigated the surface of membranes shown as SEM images (figures 11 and 12). Both membranes had local indents in their surfaces, especially the cylindrical membrane. The parallel lines indicated the fabrication process. We were, however, unable to conclude if the indents were only superficial or all through membrane channels.

The PTFE is a very hydrophobic material and has a huge water entry pressure that goes up to 620 kPa (Goldberg *et al* 1997). Even if these indents on the surface were all through channels, the water could not diffuse into the membrane at such small pressures measured as described in section 2.4.6.

The PTFE is a difficult material to machine and glue. Membranes such as silicon rubber and polyurethane have been suggested as alternative membrane materials (Arquint 1994, Varlan and Sansen 1997). However, in this study we tried to make the sensor with few parts and materials. In addition, the suggested materials except PTFE were not mechanically strong to make a robust sensor. A preferred solution could be a combination of two different membranes. For example, a PTFE membrane with rather large pores could be coated with either silicon rubber or polyurethane. Such a membrane could be both mechanically strong

and also gain a huge diffusion rate. Further research is required to examine such combinations in detail.

3.2. Sources of error

3.2.1. Electrode polarization. The moment the electrodes are in contact with the electrolyte, a relocation of ions will take place. When an AC current passes between the electrodes, the current disturbs and dislocates the ions leading to electrode polarization immittance.

There are several measuring techniques that can be applied to minimize the electrode polarization effect, such as the four-electrode measuring technique (Schwan and Ferris 1963). For the purpose of the miniaturization and easy assembly, a two-electrode measuring technique was nevertheless favored.

Another approach to minimize the error contributed from the electrode polarization immittance is the bridge geometry that we have utilized in this paper. In addition, optimizing electrode material and frequency is important to get the best results. In this way, the effect of the electrode polarization has been eliminated.

3.2.2. Stray capacitance. The stray capacitance C_s as shown in figure 1 is in parallel with the admittance of the sensor. If we denote the admittance of the electrode polarization contribution as Y_p as presented in our model (figure 1), we have

$$Y_p = G_{dc} + G_p + j\omega C_p.$$

Since there are two electrodes, the admittance for the electrode polarization and the electrolyte admittance will then be

$$Y_{pe} = \frac{G_e Y_p}{2G_e + Y_p}.$$

The total admittance of the model can then be calculated by $Y_{total} = Y_{pe} + j\omega C_s$.

If we apply an amperometric measuring method, we will obtain Y_{total} directly by measuring the current. With the lock-in amplifier, we measure the real and imaginary parts separately. By using only the real part of the Y_{total}, we measure the real part of Y_{pe} with the effect of the stray capacitance suppressed. This is, however, a theoretical assumption and in practice a too large C_s will increase the measuring uncertainty of the real part of Y_{total}. The cable type and length of the cable are therefore crucial.

3.2.3. Contamination. Contamination in the form of ions other than those produced by CO_2 decreases the sensor's sensitivity (Varlan and Sansen 1997).

The calibration curves in figures 14 and 15 show the measuring response of the sensors with different PCO_2 tensions. As predicted by the theory, the conductance was proportional to the square root of PCO_2. The signal for the planar sensor changed about 20% when PCO_2 changed from 6.0 kPa to 9.0 kPa. The cylindrical sensor had a 30% change for the same PCO_2 span. The per cent changes were smaller in the planar sensor because it was more contaminated than the cylindrical sensor.

The conductance of the sensors for 0 kPa PCO_2 could be achieved by extrapolating the calibration curves. Assuming that the channel in each sensor mostly affects the sensor conductance, the expected conductance of both sensors was about 0.4 μS and 0.3 μS for the box shaped and the cylindrical sensors, respectively. We concluded that the sensors were still contaminated even after the cleansing process.

3.2.4. Pressure and temperature. External pressure should not change the geometry of the measuring cell, since it would represent an important source of error for the conductivity measurement. In fact, if the membrane of the cylindrical sensor were an impermeable thin material the sensor could be changed to a pressure sensor.

The design of the planar sensor was in such a way that no external pressure could affect the geometry of the measuring cell. The grid supported the membrane and ensured that the external pressure did not change the measuring geometry. Thus, this was a rather difficult solution to manufacture and miniaturize. In the cylindrical design pressure sensitivity was not detected; however, it may become pressure sensitive when the membrane thickness is diminished.

Another solution was to have a hydrophilic material as a supportive spacer. This could be an easy solution for the planar macro structure but it was difficult for the cylindrical design. It may also be rather difficult to utilize such a spacer in a miniaturized sensor.

Temperature is dependent on three factors: the solubility of CO_2 in tissue and in the water inside the chamber, the mobility of the ions and the reactions for the water dissociation. When the blood supply in an organ is reduced, the temperature may decrease.

According to Butler (1982) when temperature increases from 30 °C to 37 °C, Henry's constant changes from 2.0 to 2.31 (mmol l^{-1} kPa^{-1}). For example, the reduction of temperature from 37 °C to 30 °C will increase the solubility of CO_2 resulting in a pressure change from 5.8 kPa to 5 kPa. Increasing the concentration of the dissolved PCO_2 will also increase the proton and bicarbonate concentration.

The temperature dependences of conductivity measurements are believed to be roughly 2% $°C^{-1}$ (Foster and Schwan 1989).

A temperature sensor is therefore needed to convert values to 37 °C.

3.3. Future miniaturized design

3.3.1. Miniaturizing the design. A macro sensor model does not completely characterize the actual behavior in a miniaturized form. Nevertheless, it is an indicator to understand the basic principle and functionality.

As carbon dioxide can diffuse through the living cell membrane and the tissue, a sensor can measure the PCO_2 at the surface of an organ. The planar sensor is well suited for such measurements because it is sensitive only on the side in contact with the tissue. However, fixing the sensor on the surface will be troublesome especially when the organ is moving, e.g. a beating heart. An easier way to fix the sensor is by insertion. The insertion depth can vary from organ to organ and different anatomies. A cylindrical sensor can be designed as a part of medical catheter that eases the insertion.

Depending on organ anatomy and the insertion technique, a small insertion with a tiny diameter will be less damaging to blood vessels. A miniaturized sensor allows less tissue damage, which in turn may influence PCO_2 values. Miniaturizing the sensor in its length is therefore not as important as in the cross-sectional area of the sensor. In the planar design, miniaturizing the sensor in the cross-sectional area is difficult due to the required space for the supportive grid and membrane surface area. The cylindrical design in our solution can easily be miniaturized in diameter. The membrane provides a diffusible area on its entire circumference. In contrast, the planar design has a limited membrane surface only on one side.

The cylindrical sensor may be pressure sensitive since there is less mechanical support for the membrane.

During a miniaturizing process, the channel thickness has to be kept small and the cavity volume large, to make sure that the current density at the electrode surfaces is small and evenly distributed.

3.3.2. Biocompatibility. Sensors for clinical purposes have to be biocompatible for several reasons. We categorize it into two main groups: safety and functionality. The safety issue touches the FDA protocol concerning the choice of a material that does not react in the body. The functionality of the sensor is very much dependent on its membrane properties. If the membrane is attacked by the immune system, the blockage on the membrane surface will result in a decrease of the CO_2 diffusion rate (Black 1999).

The reason that we preferred the cylindrical design was its large contact area with the tissue. If some parts of the membrane are blocked by clotting or macrophages, other parts of the membrane will still be permeable for gas diffusion keeping the sensor sensitive to CO_2.

3.3.3. Noise and preamplification. In a miniaturized sensor version, there is a need also for miniaturized cables to connect the sensor to the instruments. This means that the capacitance and cross talk will increase when the cable is miniaturized. An improved geometry design of the sensor, in addition to proper wiring and pre-amplification of the signal will minimize the stray capacitance introduced by the miniaturized cable effect. The material and the geometry of the cable chosen for the miniaturized version are crucial for the total measurement.

However, the length of the wires connecting the sensor to the instrument is also important. The longer the wire is, the closer the preamplifier has to be to the sensor.

Choosing an optimal frequency will be in practice a trade-off between capacitance coupling in the system and the electrode polarization as discussed earlier.

4. Conclusions

The results of this paper are needed to realize a miniaturized sensor to measure the PCO_2 and consequently detect ischemia in organs. The two designs that were tested and analyzed showed that both designs had advantages and disadvantages for a future miniaturization. Planar sensor is a preferred geometry for surface measurements while the cylindrical sensor is preferred for tissue insertion.

The next version of these conductivity based PCO_2 sensors is based upon the design principle as investigated in this paper.

Acknowledgments

We like to thank the instrument workshop of the Department of Physics, University of Oslo. Our special thanks to divisional engineers Sven Ivar Christiansen and Steinar Skaug Nilsen. Our thanks also go to chief engineer Sissel Jørgensen at the Centre for Materials Research, University of Oslo, for helping us with the SEM images. We are indebted to the Norwegion Research Council for financial support.

References

Arquint P 1994 Integrated blood gas sensor for pO_2, pCO_2 and pH based on silicon technology, Institute of Microtechnology, University of Neuchatel

Baker J M, Spaans E J A and Reece C R 1996 Conductimetric measurement of CO_2 concentration: theoretical basis and its verification *Agron. J.* **88** 675–82

Black J 1999 *Biological Performance of Material* (New York: Dekker) pp 10–33
Butler J N 1982 *Carbon Dioxide Equilibria and Their Applications* (Reading, MA: Addison-Wesley)
Cunningham R E and Williams R J J 1980 *Diffusion in Gases and Porous Media* (New York: Plenum)
Detemple P *et al* 1998 Microtechnology in modern health care *Med. Device Technol*. **11** 18
Foster K R and Schwan H P 1989 Dielectric properties of tissue and biological materials: a critical review *CRC Crit. Rev. Biomed. Eng*. **17** 25–104
Geddes L A, Da Costa C P and Wise G 1971 The impedance of stainless-steel electrodes *Med. Biol. Eng*. **9** 511–21
Goldberg W, Tilley M and Rudolph J 1997 *Design Solutions Using Microporous Hydrophobic Membranes* http://www.devicelink.com/mpb/archive/97/03/002.html
Grimnes S and Martinsen Ø G 2000 *Bioimpedance and Bioelectricity Basics* (New York: Academic)
Hoffman W E *et al* 1998 Measurement of ischemia by changes in tissue oxygen, carbon dioxide and pH *Surg. Neurol*. **51** 654–8
Hong X J 1996 Experimental study of arteriovenous differences in pH and partial pressure of carbon dioxide as indicators of tissue hypoxia *Blood Gas News* **5** 3–9
Jacobs P, Varlan A R and Sansen W 1995 Design optimisation of planar electrolytic conductivity sensors *Med. Biol. Eng. Comput*. **33** 802–10
Kempen L H J and Kreuzer F 1975 The CO_2 conductivity electrode: a fast responding CO_2 microelectrode *Respir. Physiol*. **24** 89–106
Koryta J, Dvorak J and Kavan L 1993 *Principles of Electrochemistry* (New York: Wiley) pp 29–39
Kvarstein G, Mirtaheri P and Tønnessen T I 2004 Detection of ischemia by PCO_2 before adenosine triphosphate declines in skeletal muscle *Crit. Care Med*. **32** 232–7
Lis K *et al* 1979 A *p*CO2 surface electrode working on the principle of electrical conductivity *Pflugers Arch*. **381** 289–91
Niggermann M, Ehrfeld W and Weber L 1999 Miniaturized plastic micro plates for applications in HTS *Microsyst. Technol*. **6** 48–53
Nunn J F 1993 *Nunn's Applied Respiratory Physiology* (Oxford: Heinemann)
Onaral B and Schwan H P 1982 Linear and nonlinear properties of platinum electrode polarization: Part1. Frequency dependence at very low frequencies *Med. Biol. Eng. Comput*. **20** 229–306
Ragheb T and Geddes L A 1990 Electrical properties of the metallic electrodes *Med. Biol. Eng. Comput*. **28** 182–6
Rolfe P 1995 Experience with invasive and non-invasive sensors for anaesthesia *Acta Anaesthesiol. Scand*. **104** 61–8
Schwan H 1968 Electrode polarization impedance and measurements in biological materials *Ann. New York Acad. Sci*. **148** 191–209
Schwan H P and Ferris C D 1963 Four-electrode null technique for impedance measurements with high resolution *Rev. Sci. Instrum*. **39** 481–3
Severinghaus J W and Brandley F 1958 Electrodes for blood PO_2 and PCO_2 determination *J. Appl. Physiol*. **13** 515–7
Siggaard-Andersen O, Gøthgen H and Fogh-Andersen N 1995 From *in vitro* to *in vivo* monitoring *Acta. Anaesthesiol. Scand*. **39** 7–13
Stow R W, Baer R F and Randall B F 1957 Rapid measurement of the tension of carbon dioxide in blood *Arch. Phys. Med. Rehabil*. **7** 646–50
Tønnessen T I 1997 Biological basis for PCO_2 as a detector of ischemia (review) *Acta Anaesthesiol. Scand*. **41** 659–69
Tønnessen T I and Kvarstein G 1996 PCO_2 electrodes at the surface of the kidney detect ischemia *Acta Anaesthesiol. Scand*. **40** 510–9
Varlan A R and Sansen W 1997 Micromachined conductimetric $p(CO_2)$ sensor *Sensors Actuators* B **55** 309–15